Optics Letters

Luminescent solar concentrator efficiency versus edge solar cell coverage

Xi Lu, Jingjian Zhou, Madhuri Jash, and Ilya Sychugov*

Department of Applied Physics, KTH – Royal Institute of Technology, Stockholm 11419, Sweden
**ilyas@kth.se*

Received 1 June 2023; revised 14 July 2023; accepted 15 July 2023; posted 17 July 2023; published 2 August 2023

This Letter introduces an analytical approach to estimate the waveguiding efficiency of large-area luminescent solar concentrators (LSCs), where the edges are covered by a varied number of mirrors and solar cells. The model provides physically relevant description in the whole range of optical (absorption, scattering) and geometrical (size) parameters of rectangular LSCs. A 19×19 cm^2 silicon quantum dot-based LSC has been fabricated to verify the theory. Within an experimental error, the predicted waveguiding efficiency matched well the measured one. A critical LSC size, beyond which a part of the device turns inactive, has been determined as N/α for N attached solar cells (one or two) and LSC material absorption coefficient α. This model provides a straightforward waveguiding analysis tool for large-area LSCs with different structural parameters relevant for both high concentration ratio and glazing applications.

https://doi.org/10.1364/OL.496595

Luminescent solar concentrators (LSCs) were first introduced in the early 1970s and were based mainly on organic dyes as fluorophores [1]. By waveguiding their sunlight-generated photoluminescence (PL) inside the LSCs, the device concentrates light harvested by large surface areas to small edges through PL total internal reflection. Recently, LSCs became attractive again due to their semi-transparency, thus of potential interest for a building-integrated photovoltaic (BIPV), commonly described as "solar windows" [2,3]. The number of edges covered by solar cells (sc) versus mirrors varies depending on the device utilization: from a single solar cell in the original concept to half or full perimeter coverage for solar windows.

The main operational principle of an LSC is the total internal reflection, where PL is trapped inside the device until it reaches the solar cell at the edges. The toolbox of light-converting fluorophores by now has expanded from organic dyes [4] to semiconductor quantum dots [2], rare-earth ions [5], and metal nanoclusters [6]. In addition to the performance of the chosen fluorophore, i.e., photoluminescence quantum yield (PLQY) and its reabsorption suppression (Stokes shift), the total efficiency of the LSC device also highly depends on the waveguiding efficiency. In fact, the waveguiding part is the most difficult to evaluate for LSC efficiency prediction, as it is a complex function of different loss mechanisms (absorption, scattering, etc.)

Many efforts have been devoted to estimating the waveguiding efficiency of the LSC devices [7–9]. Ideally, one needs a model that can accurately predict the waveguiding efficiency for different area devices, in particular for large-area LSCs. The latter is not easy to measure experimentally due to the limitation like the need of a correspondingly large solar simulator [10]. As a result, it makes simple mathematical extrapolation from the available small-area LSCs data not very reliable. From the theory side, phenomenological models have mainly been employed previously, such as a polynomial fitting to extensive Monte-Carlo simulations [8,9,11]. Although useful as a first-order approximation, those are void of physical meaning and cannot explicitly reveal transitions between different device operation regimes with increasing geometries.

In this Letter, we introduce an analytical model to describe the waveguiding efficiency of large-area LSCs, where the four edges are covered by a varied number of mirrors and solar cells. These full and simple analytical formulas are not only a straightforward tool for waveguiding efficiency calculation, but also can be used to evaluate the device performance in different material systems for the whole range of αL, where L (cm) is the device length, and α (cm^{-1}) is an attenuation coefficient (e.g., matrix absorption coefficient α_{mx}). We discuss the physical meaning of the formula, compare our model with the phenomenological expression from [8], and outline reasons for deviations. Importantly, the model predicts a linear dependence in the log-log scale for large αL, which reveals a different waveguiding regime in large-area LSC devices, corresponding to signal contribution from a limited area. Explicit values for critical LSC device sizes before the onset of this less favorable waveguiding regime are presented. The model was experimentally verified by a set of measurements on a 19×19 cm^2 silicon quantum dot-based LSC, where all relevant losses were quantitatively considered, validating the theory without any fitting parameters.

We start by considering a rectangular LSC with two edges covered with solar cells and two others with mirrors (Fig. 1, inset). The key idea of this work is that for an isotropic light emitter placed inside the slab, this geometry is equivalent to two infinitely long solar cells, as far as the optical path is concerned.

Previously, we have shown that the general expression for the waveguiding efficiency of rectangular LSCs with full perimeter

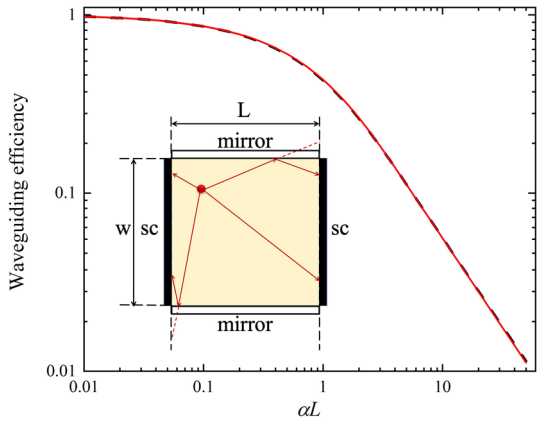

Fig. 1. Waveguiding efficiency for a rectangular LSC with two mirrors from Eq. (2) (red line) and from the general formula [Eq. (1), black dashes line, w = 50000 cm]. Inset shows device schematics.

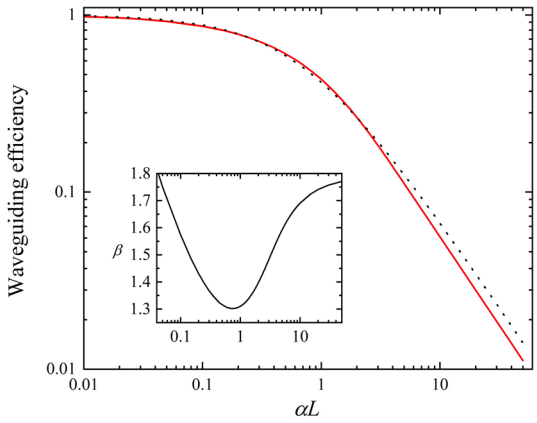

Fig. 2. Comparison of Eq. (2) (red line) with the phenomenological equation $(1+\beta\alpha L)^{-1}$, $\beta = 1.4$ (black dotted line). Correct values of β are shown in the inset.

coverage by solar cells is [7]

$$f_{4sc}(\alpha L,\alpha w)=\frac{2((L+w)\alpha k-(kd\alpha+1)e^{-kd\alpha}+e^{-kL\alpha}+e^{-kw\alpha}-1)}{k^2Lw\pi\alpha^2}-I_1-I_2$$
$$I_1=\frac{2}{kw\pi}\int_{kw}^{kd}\frac{\sqrt{x^2-k^2w^2}}{x}e^{-\alpha x}dx \quad , \quad I_2=\frac{2}{kL\pi}\int_{kL}^{kd}\frac{\sqrt{x^2-k^2L^2}}{x}e^{-\alpha x}dx \tag{1}$$

where L and w are the length and the width of the rectangular, $d=\sqrt{L^2+w^2}$ is the diagonal length, and k is a coefficient for 3D geometry, which for the glass–plastic interface is $k\approx 1.14$ [7]. Equation (1) has been verified through numerical modeling by other groups [9,11].

Then, for the infinitely wide device ($w \gg L, w\to\infty$), one can expand the general formula in Eq. (1) by a small parameter L/w (see derivations in Supplement 1), and the waveguiding efficiency becomes a function of a single parameter αL,

$$f_{2sc}(\alpha L)=\frac{2(1-e^{-\alpha kL})}{\alpha kL\pi}+\frac{(\pi-2)e^{-\alpha kL}}{\pi}-\frac{\alpha kL}{\pi}E_1(\alpha kL), \tag{2}$$

where E_1 is a special function called "exponential integral". In Fig. 1, we show that Eqs. (1) and (2) are indeed equivalent for a very wide LSC device, thus confirming validity of the derived integral-free expression.

A simple expression of Eq. (2) allows detailed waveguiding efficiency analysis. From Eq. (2), its trend for large αL can be immediately evaluated as $f_{2sc\infty}=2/\alpha kL\pi$ (due to quickly decaying exponential and exponential integral terms). It is indeed seen as a straight line in the log-log scale in Fig. 1, and the same trend was presented for large device in one of the original LSC reports [12]. It is also obvious from Eq. (2) that for $\alpha L\to 0$, the function f_{2sc} becomes unity, as expected for a no-loss scenario.

Now we can compare Eq. (2) with a phenomenological expression $(1+\beta\alpha L)^{-1}$ with a parameter $\beta\approx 1.4$, obtained by polynomial fitting of extensive Monte Carlo simulations [8]. In Fig. 2, this function is compared with Eq. (2) and deviation at large αL is visible. Strictly speaking, the parameter β is not a constant, but depends on αL. By solving the equation $f_{2sc}(\alpha L)=(1+\beta\alpha L)^{-1}$, the actual values of β as a function of αL can be obtained (shown in Fig. 2, inset). It is seen that β saturates for $\alpha L\to\infty$ at $\beta_\infty=k\pi/2\approx 1.79$, which is why a value of 1.8 was suggested for this range in [8].

The main advantage of Eq. (2) is, however, not a more accurate waveguiding efficiency description for $\alpha L\to\infty$, but the analysis facility. Indeed, for large values of αL, it is only the area next to the solar cells that contribute to the waveguiding efficiency, while the part in the middle of the device become inactive (extinct PL). Then the useful area in such a case can be estimated as $2\alpha^{-1}w$ (two rectangles close to solar cells), while the total area is Lw. In general, the waveguiding efficiency is proportional to the useful fraction of the total area, so it scales here as $2/\alpha L$. Therefore, the analytical expression at large αL range, $f_{2sc\infty}=2/\alpha kL\pi$ reveals an inferior waveguiding regime, where the central part of the device is no longer active (straight line in the log-log scale).

Thus, it is important to identify a transition point where the function $f_{2sc}(\alpha L)$ turns linear in the log-log scale. From Fig. 1, we can set a numerical limit for the LSC with two edges covered by solar cells approximately at $\alpha L=2$. Here the deviation of the straight line from f_{2sc} is only approximately 5%, which can be within experimental measurement error. So, for a typical polymer/glass matrix (PMMA, OSTE, low-iron glass) with an absorption coefficient of 0.04–0.05 cm^{-1}, the maximum mirror length translates to the value $L_{max}=40-50$ cm. This result is not straightforward from the phenomenological description method.

Now we turn to a rectangular-shaped LSC with only one edge covered by a fully absorbing photodetector and the rest with mirrors. In fact, it was one of the initially proposed configurations to enhance the collected light concentration about half-a-century ago [12], for which efficiency limits are still being explored numerically today [13]. From the same optical path arguments, it can be shown that for one side solar cell and three side mirrors, the geometry is equivalent to the case of two infinite solar cells separated by mirrors with a length of $2L$, $f_{1sc}(\alpha L)=f_{2sc}(2\alpha L)$:

$$f_{1sc}(\alpha L)=\frac{2(1-e^{-2\alpha kL})}{2\alpha kL\pi}+\frac{(\pi-2)e^{-2\alpha kL}}{\pi}-\frac{2\alpha kL}{\pi}E_1(2\alpha kL). \tag{3}$$

Thus, this formula, whose asymptote was shown in the original work of Weber and Lambe [12], has never explicitly been revealed until now. From Eq. (3), the asymptote for large αL yields $f_{1sc\infty}=1/\alpha kL\pi$, which is two times lower than in the previous case. It can be understood simply from the fact that in this regime, reflected light does not reach the detector and only

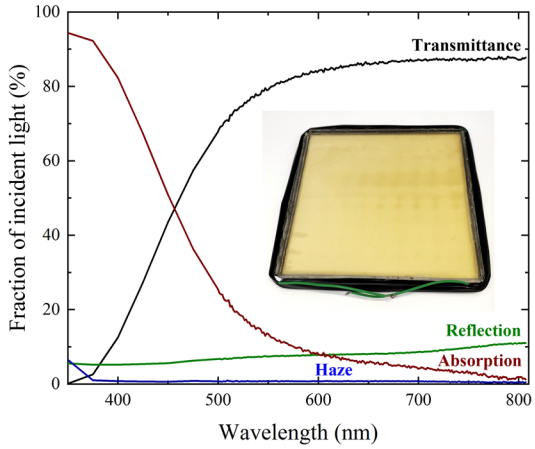

Fig. 3. Transmittance, absorption, reflection, and haze spectra of the used LSC device. Inset is a photo of the used 19×19 cm^2 LSC device.

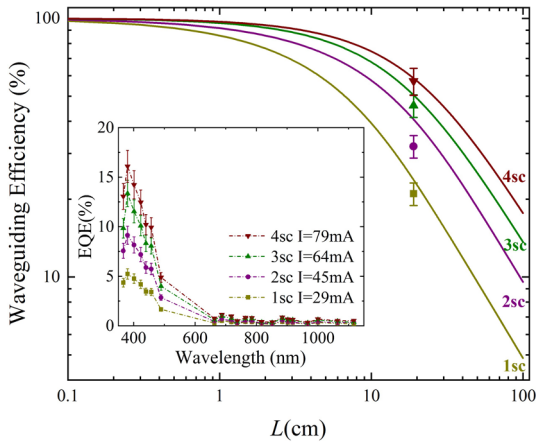

Fig. 4. Waveguiding efficiency of the device in the cases of different numbers of edges covered by solar cells: 1, 2, 3, and 4 edges (the remaining edges are covered by mirrors). Lines are from Eq. (5) and points are from the experiment [Eq. (6)]. Inset are external quantum efficiency and short circuit current of the device.

emitters close to the collecting edge contribute. So already at $\alpha L = 1$, some areas of the LSC in this design stop contributing. For typical matrix materials introduced above, the maximum mirror length for the proper LSC waveguiding regime is then only $L_{max} = 20 - 25$ cm. Note that this is the upper limit, in the presence of scattering and re-absorption, L_{max} will be even lower. Thus, it becomes clear that the matrix absorption critically limits its useful mirror-LSC sizes, and materials such as ultra-low iron glass ($\alpha \leq 0.01$ cm^{-1}) or fluorine-based polymers are needed for large-area LSCs with mirrors. Other models based on mathematical extrapolation from the measured small-area LSCs data, or polynomial fitting to simulations, cannot easily reveal such variations in the waveguiding mechanism.

To complete the description, a rectangular LSC with three side solar cells and one side mirror can also be considered. In this case, the system is similar to a rectangle with fully covered perimeter with a double length. Then the waveguiding efficiency is not a function of a single parameter. It can be expressed from the general formula of Eq. (1) as

$$f_{3sc}(\alpha L, \alpha w) = f_{4sc}(2\alpha L, \alpha w). \tag{4}$$

After the theoretical basis has been established, we move on to the experimental validation. A 19×19 cm^2 LSC device was fabricated to verify our analytical approach, following the procedure which can be found elsewhere [14]. A 3-mm-thick off-stoichiometry thiol-ene (OSTE) polymer interlayer uniformly mixed with luminescent Si quantum dots (QDs; PL peak position ~ 870 nm, as shown in Fig. S1 in Supplement 1, PLQY ~ 50%) was embedded in between two 2-mm-thick glass sheets. A photo and general optical characterization of this device are shown in Fig. 3. Absorption, reflection, transmittance, and haze were measured by a home-built integrating sphere setup. Short-circuit currents and external quantum efficiencies (EQEs) were measured with a large-area (25×25 cm^2) AM1.5G solar simulator, where EQE(λ) is the ratio of generated electrons by the edge solar cells to incident photons on the device top area.

To measure all the configurations mentioned above, the initial device had three mirror-covered edges (attached by a polymer without an air gap) and one solar cell-covered edge. Then the mirrors (metal-coated plastic bars) were replaced by solar cells one by one. "Roofs" (5-mm-wide black paper stripes) covered the top of the device edges for preventing any direct illumination on the solar cell. Ideally, only the portion of sunlight absorbed by Si QDs should contribute to the generated electrons for an intrinsic LSC performance evaluation. To verify this, EQEs were measured. As can be seen in Fig. 4, inset, EQEs are indeed close to zero above 650 nm, implying almost all the measured photocurrent (I-V curves shown in Fig. S2 in Supplement 1) is formed by the photons from the luminescent Si QDs, and not from the direct light (EQE curve follows Si QD absorption curve, cf. Fig. S1 in Supplement 1).

For more relevant comparison with theory, we note that in practical situations, scattering, re-absorption and matrix absorption losses are all present. In this case, the waveguiding efficiency for N solar cell coverage becomes [7]

$$g_{Nsc} = \frac{f_{Nsc}(\alpha_{mx} + \alpha_{re} + \alpha_{sc})}{1 - \frac{\delta\alpha_{sc} + \delta\alpha_{re} \cdot QY}{\alpha_{mx} + \alpha_{re} + \alpha_{sc}}(1 - f_{Nsc}(\alpha_{mx} + \alpha_{re} + \alpha_{sc}))}, \tag{5}$$

where δ is the probability to scatter into a waveguiding mode (0.75 for glass/plastic slab in air) and QY is the PLQY. As reported previously [14], the average matrix absorption coefficient α_{mx} is 0.045 cm^{-1} for OSTE and of similar value for the low-iron glass applied here in the Si QD PL range. Reabsorption coefficient at the PL peak for Si QDs α_{re} is 0.007 cm^{-1}, and the scattering coefficient α_{sc} can be estimated by haze measurement, which is 0.014 cm^{-1} in our device. Experimental details of the extinction coefficients can be found in Supplement 1 (including Figs. S3–S5 in Supplement 1). Note that function g_{Nsc} depends no longer on just one (αL), but several independent variables (the effect of each independent variable is analyzed in Fig. S6 in Supplement 1).

Finally, the short-circuit current can be presented as

$$I = \Phi_A L^2 \delta \cdot QY \cdot g_{Nsc} \cdot EQE_{sc} \cdot A, \tag{6}$$

where Φ_A is the number of the absorbed photons (cm^{-2}s^{-1}) (obtained from the measured absorption curve and solar photon spectrum), and EQE_{sc} is the EQE of solar cells at the PL peak wavelength of the Si QDs (~ 0.9). Here, A is the fraction of active solar cell area (as shown in Fig. S7 in Supplement 1) to the entire edge area (~ 0.9). We used eight solar cells each containing four p-n junctions connected in parallel for every edge (KXOB25-03X4F, Anysolar). Experimental [Eq. (6),

points] and theoretical [Eq. (5), lines] values of g_{Nsc} are plotted in Fig. 4 for the 19×19 cm^2 device.

As seen, the experimental data match well with the predicted values without any fitting parameters. However, there is still a slight systematic error rendering all data points somewhat below theoretical curves. In particular, compared with the 3sc and 4sc cases, the measured waveguiding efficiencies of 2sc and 1sc are further away from the theoretical predictions. We have two hypotheses regarding this: the first one is because the mirrors may not be reflecting completely or vertically to the active layer leading to additional losses; the other possible reason is that, in our device, there are some non-uniformities, such as higher haze areas. This will cause a higher scattering loss when the luminescence light propagates through those regions. Moreover, the waveguiding efficiency in the 2sc case will be affected by these two imperfections together. By contrast, in the 1sc case, the extinction loss is already high (due to the long light path), while in the 3sc case, the mirror-reflected light contribution is minor. Therefore, the experiment error in the 2sc case appears to be the most significant. We also note from Fig. 4 that for the 1sc case, the 19×19 cm^2 device indeed already approaches its critical size (straight line regime in log-log scale).

To conclude, we present an analytical model for the LSCs for different solar cell edge-coverage. Compared with existing models based on extrapolation of small-area LSCs experimental results, numerical simulations, or polynomial fittings, this methodology is not only more accurate, but also contains physical information, making it possible to establish criteria for largest meaningful LSC sizes with attached mirrors. This critical LSC size can be expressed as $L_{crit} = N/\alpha$ for $N = 1$ or 2 solar cells covering the LSC edges for the absorption coefficient α. The proposed analytical approach was successfully verified by a 19×19 cm^2 Si QDs-based LSC, with results confirming the theory within the experimental error.

Funding. Energimyndigheten (46360-2).

Acknowledgment. X.L. acknowledges funding support from the China Scholarship Council (CSC).

Disclosures. The authors declare no conflicts of interest.

Data availability. Data underlying the results presented in this paper are not publicly available at this time but may be obtained from the authors upon reasonable request.

Supplemental document. See Supplement 1 for supporting content.

REFERENCES

1. G. Keil, Methods **89**, 111 (1970).
2. F. Meinardi, S. Ehrenberg, L. Dhamo, F. Carulli, M. Mauri, F. Bruni, R. Simonutti, U. Kortshagen, and S. Brovelli, Nat. Photonics **11**, 177 (2017).
3. N. S. Makarov, D. Korus, D. Freppon, K. Ramasamy, D. W. Houck, A. Velarde, A. Parameswar, M. R. Bergren, and H. Mcdaniel, ACS Appl. Mater. Interfaces **14**, 29679 (2022).
4. A. Sanguineti, M. Sassi, R. Turrisi, R. Ruffo, G. Vaccaro, F. Meinardi, and L. Beverina, Chem. Commun. **49**, 1618 (2013).
5. T. Wang, J. Zhang, W. Ma, Y. Luo, L. Wang, Z. Hu, W. Wu, X. Wang, G. Zou, and Q. Zhang, Sol. Energy **85**, 2571 (2011).
6. K.-B. Cai, H.-Y. Huang, P.-W. Chen, X.-M. Wen, K. Li, J.-L. Shen, K.-P. Chiu, and C.-T. Yuan, Nanoscale **12**, 10781 (2020).
7. I. Sychugov, Optica **6**, 1046 (2019).
8. V. I. Klimov, T. A. Baker, J. Lim, K. A. Velizhanin, and H. McDanielM, ACS Photonics **3**, 1138 (2016).
9. T. A. de Bruin and W. G. J. H. M. van Sark, Sol. RRL **7**, 2200787 (2023).
10. J. Zhou, J. Huang, and I. Sychugov, Opt. Lett. **47**, 4985 (2022).
11. Z. Zheng, Y. Zhang, X. Cao, G. Gu, Y. Tian, and X. Zhang, Opt. Lett. **47**, 4367 (2022).
12. W. H. Weber and J. Lambe, Appl. Opt. **15**, 2299 (1976).
13. J. S. van der Burgt, D. R. Needell, T. Veeken, A. Polman, E. C. Garnett, and H. A. Atwater, ACS Appl. Mater. Interfaces **13**, 40742 (2021).
14. J. Huang, J. Zhou, E. Jungstedt, A. Samanta, J. Linnros, L. A. Berglund, and I. Sychugov, ACS Photonics **9**, 2499 (2022).

Supplemental Document

Optics Letters

Luminescent solar concentrator efficiency versus edge solar cell coverage: supplement

Xi Lu, Jingjian Zhou, Madhuri Jash, and Ilya Sychugov*

Department of Applied Physics, KTH – Royal Institute of Technology, Stockholm 11419, Sweden
*ilyas@kth.se

Supplement DOI: https://doi.org/10.6084/m9.figshare.23695116

Parent Article DOI: https://doi.org/10.1364/OL.496595

Supporting Information

Luminescence solar concentrator efficiency versus edge solar cell coverage

XI LU,[1] JINGJIAN ZHOU,[1] MADHURI JASH,[1] ILYA SYCHUGOV[1,*]

[1]Department of Applied Physics, KTH – Royal Institute of Technology, Stockholm 11419, Sweden
**Corresponding author: ilyas@kth.se*

1. Derivation of expression for the waveguiding efficiency of a rectangular LSC with two edges covered with solar cells

Starting from Eq.(1), we consider an infinite slab with with $w \to \infty$, which corresponds to an LSC with two mirrors and two fully absorbing solar cells at the opposite edges. Here we show that in this case the general formula above can be replaced by an integral-free expression as a function of only one parameter.

The first term in Eq.(1) can be simplified using $L \ll w$, $w \to \infty$, and $d \approx w$ as

$$\frac{2(w\alpha k(1-e^{-kw\alpha})+L\alpha k+e^{-kL\alpha}-1)}{k^2 Lw\pi\alpha^2} \approx \frac{2}{kL\pi\alpha}$$

The first integral I_1 is negligible because $d \approx w$. Second integral can be expanded by small parameter $kL/x \ll 1$ because only for those x this expression is different from zero:

$$I_2 = \frac{2}{kL\pi}\int_{kL}^{kw}\sqrt{1-(kL/x)^2}e^{-\alpha x}dx \approx \frac{2}{kL\pi}\int_{kL}^{kw}\left(1-\frac{1}{2}\left(\frac{kL}{x}\right)^2-\frac{1}{8}\left(\frac{kL}{x}\right)^4-\ldots\right)e^{-\alpha x}dx$$

Taking these integrals and leaving only first-order terms for L:

$$I_2 \approx \frac{2e^{-\alpha kL}}{kL\pi\alpha}-\frac{(\pi-2)e^{-\alpha kL}}{\pi}+\frac{\alpha kL}{\pi}E_1(\alpha kL)$$

where E_1 is an exponential integral (a commonly encountered special function):

$$E_1(\alpha kL) = \int_{\alpha kL}^{\infty}\frac{e^{-\xi}}{\xi}d\xi$$

The factor for the second term comes from the converging series:

$$\sum_{k=1}^{\infty}\frac{\Gamma(k-\frac{1}{2})}{\sqrt{\pi}\cdot\Gamma(k+1)\cdot(2k-1)} = \pi-2$$

where Γ is a gamma function.

Finally, combining with the expression for the first term the result is:

$$f_{2sc}(\alpha L) = \frac{2(1-e^{-\alpha kL})}{kL\pi\alpha}+\frac{(\pi-2)e^{-\alpha kL}}{\pi}-\frac{\alpha kL}{\pi}E_1(\alpha kL)$$

2. Absorption and emission spectrum of Si QDs

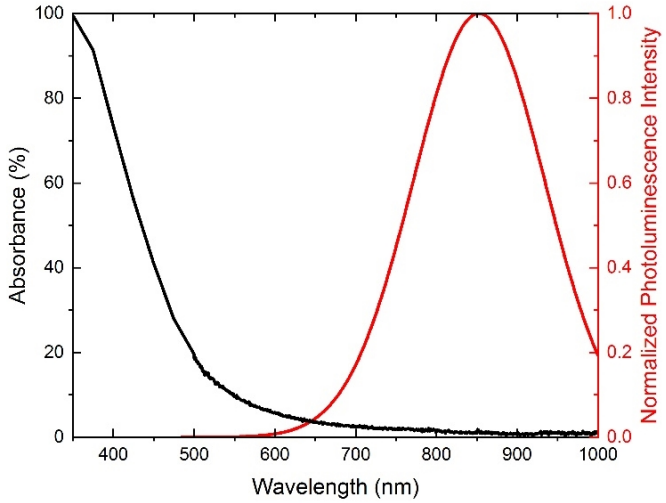

Fig. S1 UV-Vis absorption (black) and fluorescence (red) spectra of Si QDs in OSTE. The fluorescence spectrum was obtained in an integrating sphere with an excitation wavelength of 440nm by Gaussian fitting to the measured curve.

3. Photovoltaic Measurements

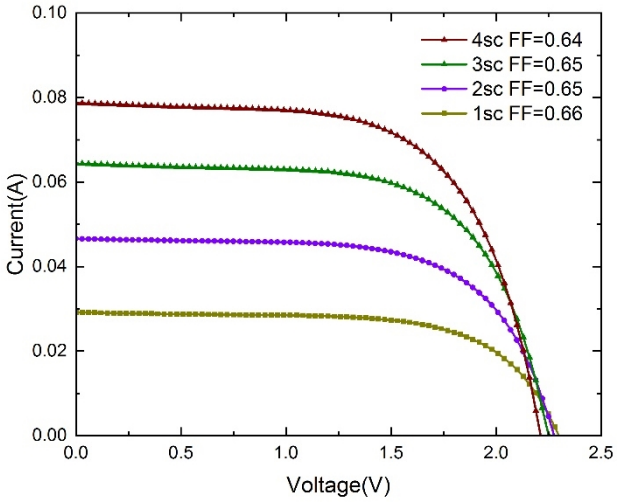

Fig. S2 *I-V* characteristic curves and the fill factor(FF) of the LSC under standard one sun (1000 W/m^2 in irradiance)

4. Extinction coefficients measurements

4.1 Absorption coefficient

Matrix absorption coefficient was measured using a power meter, as illustrated in Fig. S3. A laser-driven xenon plasma white-light source (Energetiq EQ-99) coupled with a tunable monochromator (SP2150i, Princeton Instruments) was used as a light source. An incident filter (FF01-650/SP-25) is used to remove half-wavelength peak for measurements above 700nm. All the samples (glass and OSTE film) are slightly tilted to the incident beam fiber (a few degrees), for directing two interface reflections away from the detector. The transmitted light was collected by the optical power meter. To reduce noise, the average of multiple measurements is used.

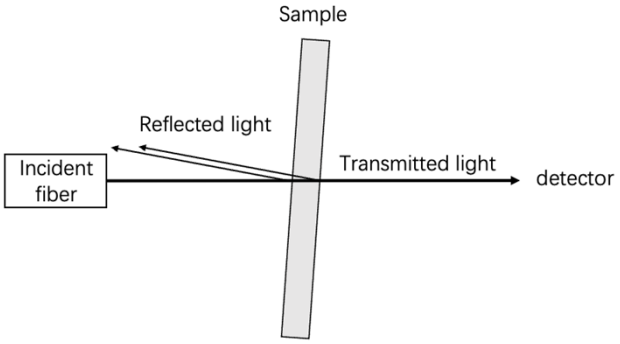

Fig. S3 Illustration of absorption measurement

If I_0 is the incident light intensity, and I_{trans} is the detected transmitted light intensity, then:

$$\frac{I_{trans}}{I_0} - R = \exp(-\alpha_{mx} \cdot d)$$

where $R=r+(1-r)*r$ is the total reflection of double glass/air interfaces (~ 8%), the exact reflection r can be calculated from matrix refractive index n_1 and n_2. This method is valid in the absence of scattering contribution to the total extinction (optically clear samples).

The measured absorption coefficient of several types of glass, OSTE, and PMMA is shown in [1] as reported previously (in supporting information).

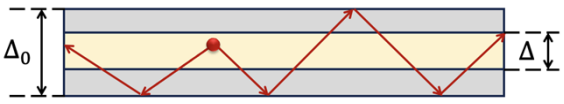

Fig. S4 Illustration of light propagation in the LSC with a triplex configuration

In the triplex configuration of our LSC, the nanocomposite is laminated between two sheets of borosilicate glass. As shown in Fig. S4, the light propagates through both glass and OSTE, therefore, the effective absorption coefficient of the LSC can be estimated as:

$$\alpha_{mx} = \frac{\Delta}{\Delta_0}\alpha_{mx\_OSTE} + \frac{\Delta_0 - \Delta}{\Delta_0}\alpha_{mx\_glass}$$

To conclude, the average matrix coefficient α_{mx} is around 0.045 cm^{-1} at the PL peak wavelength (870 nm) for used Si QDs embedded in a 3 mm OSTE layer between two 2mm thick glass layers.

4.2 Reabsorption coefficient

The reabsorption coefficient α_{re} here is estimated as the absorption coefficient for Si QDs at 870 nm, corresponding to the PL maximum. Direct extinction measurements are difficult, because at this wavelength for Si QD composites the matrix absorption and the scattering may also contribute. So we used measurements in the visible range, where extinction is dominated by Si QD absorption, to find QD concentration. Then, using known elementary cross-sections, we recalculated values for the NIR range.

For optically thin sample (exponent can be expanded in Taylor series), the measured absorbance can be defined as [2]:

$$A_e = \alpha_{re\_QD} \cdot d = \sigma \cdot C_v \cdot d$$

Where $A_e = -ln(1 - f_{abs})$ is absorbance with natural logarithm, f_{abs} is the measured absorption fraction corrected by blank OSTE as a reference, α_{re_QD} is the re-absorption coefficient, σ is the absorption cross-section, C_v is the volume concentration.

As shown in table S1, volume concentration C_v is calculated through the measured absorption fraction at 450 nm, and confirmed by measured absorption fraction at 500 nm.

Table S1. Parameters used in the calculations of volume concentration with different incident wavelength

Wavelength (nm)	Absorption fraction $\boldsymbol{f_{abs}}$	Absorbance $\boldsymbol{A_e}$	Absorption cross section $\boldsymbol{\sigma}$ (cm^2)	Volume concentration $\boldsymbol{C_v}$ (cm^{-3})
450 nm	0.51	0.71	2.4×10^{-16}	9.9×10^{15}
500 nm	0.25	0.29	1.2×10^{-16}	8.1×10^{15}

Absorption cross section at 870 nm of Si QDs similar in size to ours is around 1.9×10^{-18} cm^2 [2], which means that the reabsorption coefficient of our Si QDs with the volume concentration of 9×10^{15} is around 0.018 cm^{-1}.

Similar to the the matrix absorption coefficient, the effective reabsorption coefficient of the LSC can be estimated as:

$$\alpha_{re} = \frac{\Delta}{\Delta_0}\alpha_{re\_QD} + \frac{\Delta_0 - \Delta}{\Delta_0}\alpha_{re\_glass}$$

Due to the absence of reabsorption in the glass (free from QDs), the reabsorption coefficient α_{re} of used LSC is 0.007 cm^{-1}.

4.3 Scattering coefficient

The scattering coefficient is measured by a home-built integrating sphere for the whole device, as illustrated in Fig. S5.

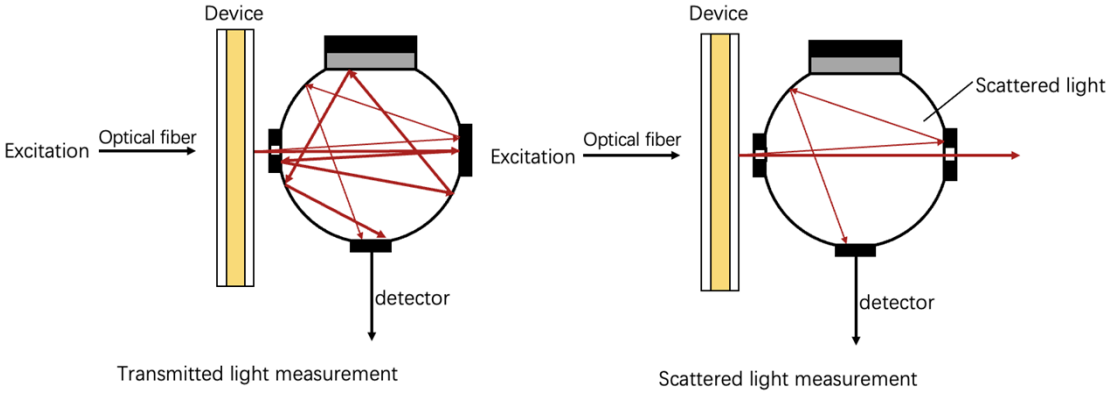

Fig. S5 Illustration of scattering measurement

The incident light at 870 nm was selected for scattering measurement, corresponding to the Si QDs PL peak position. A flange at the back side is used to ensure that only scattered light at an angle greater than 2.5° from normal was collected by the integrated sphere, then:

$$\frac{I_{sc}}{I_{trans}} = \exp(-\alpha_{sc} \cdot d)$$

Where I_{sc} is the detected scattered light. I_{sc}/I_{trans} is also the definition of haze.

In contrast to the absorption and reabsorption coefficient, the obtained scattering coefficient is already the average value of the device. As shown in Fig.3 the haze of our device at 870 nm is around 1%, therefore the scattering coefficient α_{sc} is 0.014 cm^{-1} in our device.

5. Effect of different types of waveguiding losses

We have illustrated how the waveguiding efficiency for Si QD device considered here will change in case of doubling of different loss parameters. It is clear that the matrix absorption, Fig. S6 (b), has the strongest limiting effect. QY does not have such a big effect here, which can be attributed to low re-absorption in Si QDs.

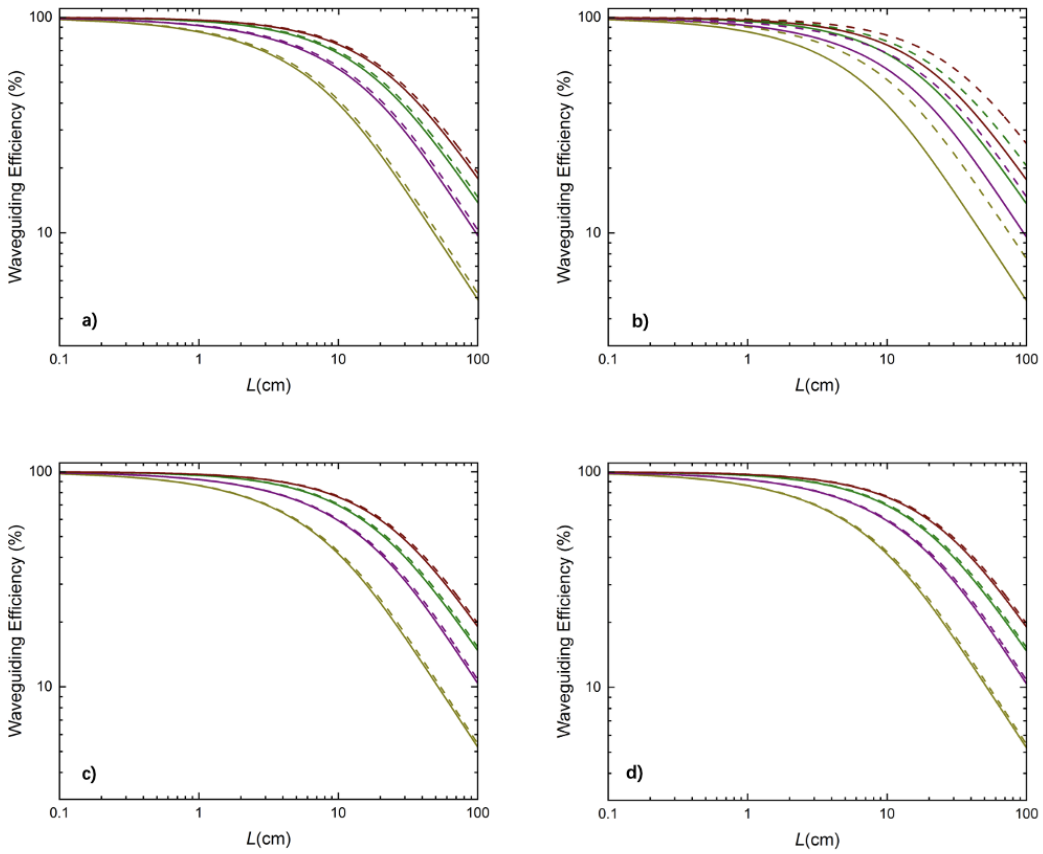

Fig. S6 Waveguiding efficiency of the device of different numbers of edges covered by solar cells (red-4sc, green-3sc, purple-2sc, yellow-1sc) under different parameters. a) solid line - PLQY = 50%, dashes line - PLQY = 90%. b) solid line - α_{mx} = 0.045 cm^{-1}, dashed line - α_{mx} = 0.024 cm^{-1}. c) solid line - α_{re} = 0.007 cm^{-1},dashed line - α_{re} = 0.003 cm^{-1}. d) solid line - α_{sc} = 0.014 cm^{-1},dashed line - α_{sc} = 0.007 cm^{-1}

6. Fraction of active solar cell area

The solar cell (KXOB25-03X4F, Anysolar) surface is illustrated in Fig. S7, the active solar cell area is the full surface minus inter-solar cell gaps, top, side and bottom electrodes.

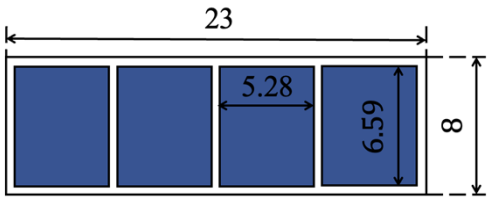

Fig. S7 Illustration of solar cell surface (mm)

[1] Huang, J., et al. "Triplex Glass Laminates with Silicon Quantum Dots for Luminescent Solar Concentrators." Solar RRL 4: 2000195. (2020).

[2] Valenta, J., et al. "Determination of absorption cross-section of Si nanocrystals by two independent methods based on either absorption or luminescence." Applied Physics Letters 108(2). (2016).